

THE RADIO SOURCE AND BIPOLAR NEBULOSITY IN THE SEYFERT GALAXY NGC 3516

TAKAMITSU MIYAJI AND ANDREW S. WILSON

Astronomy Department, University of Maryland, College Park, MD 20742

AND

ISMAEL PÉREZ-FOURNON

Instituto de Astrofísica de Canarias, 38200 La Laguna, Tenerife, Spain

Received 1991 May 17; accepted 1991 July 22

ABSTRACT

We present the results of radio continuum (20 and 6 cm) and optical emission-line ($H\alpha$ + $[N\text{ II}] \lambda\lambda 6548, 6584$ and $[O\text{ III}] \lambda 5007$) imaging observations of the type 1 Seyfert galaxy NGC 3516. These observations were obtained with the VLA and the William Herschel Telescope and are deeper and of higher resolution than earlier ones. The radio maps reveal an elongated, one-sided, curved structure, which comprises a series of small-scale “blobs” and extends up to 4 kpc from the nucleus. This radio structure is aligned and cospatial with one side of the double-sided and highly symmetric Z-shaped emission-line structure. We argue that these morphological features are associated with a bipolar, gaseous outflow from the nucleus of NGC 3516. The radio “blobs” are elongated roughly *perpendicular* to the apparent local direction of the outflow, a result which we interpret in terms of synchrotron emission from outflow-driven shock waves. For one such “blob,” the associated optical emission-line feature is displaced slightly toward the nucleus, suggesting that the line emission originates in the postshock cooling zone. There is an approximate equality between relativistic and thermal pressures in much of the nebulosity. The apparent bending of the outflow may reflect either collision with the rotating interstellar gas, or gravitationally induced trajectories in a low-velocity outflow, or precession of the nuclear axis. The direction of the present axis of the putative collimating nuclear disk is indicated by both the extended radio continuum and line emission on the smallest resolved scales (400 pc), and by the optical continuum polarization of the nucleus. Last, we note a very elongated emission-line feature about 3.3 kpc from the nucleus, that “points” toward the nucleus and is well aligned with the present nuclear axis. It is suggested that this feature represents ambient interstellar gas photoionized by a narrow beam of radiation (“blazar-like”?) from the nucleus. Such emission-line structures may be useful probes of “blazars” when the jet is not directed toward Earth.

Subject headings: galaxies: individual (NGC 3516) — galaxies: jets — galaxies: nuclei — galaxies: Seyfert — galaxies: structure — radio continuum: galaxies

1. INTRODUCTION

Radio studies of Seyfert galaxies with the VLA have revealed well-resolved, extended structures in about half the galaxies mapped (e.g., Ulvestad & Wilson 1984a, b, 1989). Most of these well-resolved galaxies exhibit linear radio structures of extent several hundred parsecs to a few kiloparsecs. These linear structures are best interpreted in terms of collimated outflow of radio-emitting plasma from the active nuclei. It is also found that the linear radio sources are well aligned and cospatial with the high-excitation extended emission-line nebulosities (Wilson 1987; Haniff, Wilson, & Ward 1988; Whittle et al. 1988). There are also correlations between radio power and both $[O\text{ III}] \lambda 5007$ luminosity and line width (e.g., Wilson & Willis 1980; Heckman et al. 1981; Whittle 1985). The nature of these close associations between relativistic and thermal gases is not well understood. In many objects, the ultraviolet photons responsible for ionizing the extended nebulosities appear to escape from the nucleus anisotropically and preferentially along and around the radio axis (e.g., Antonucci & Miller 1985; Wilson, Ward, & Haniff 1988; Tadhunter & Tsvetanov 1989). It may also be that the *rates* of escape of radio-emitting plasma and ionizing photons from the nucleus are correlated, because these two rates are regulated by the same processes (Osterbrock 1978). Other possible effects coupling the radio- and line-emitting gases include interactions between jets or

plasmoids and line-emitting clouds, acceleration of cosmic rays and/or amplification of magnetic field by the thermal cloud motions, and relaxation to pressure equality (see Whittle 1989 for recent review).

The directions of nuclear optical polarization tend to be aligned with the radio structures in Seyfert 1's and perpendicular to them in Seyfert 2's (Antonucci 1983, 1984). A recent survey by Brindle et al. (1990) using a larger sample did not confirm the parallel alignment in Seyfert 1's, however. The perpendicular relationship in Seyfert 2's can be easily understood in terms of scattering of the continuum light from a central source hidden inside a thick torus (Antonucci 1983, 1984; Antonucci & Miller 1985). The nature of the possible radio axis—optical polarization alignment in Seyfert 1's is less clear.

To clarify the underlying physical processes responsible for the general phenomena described above, detailed studies of individual galaxies are important. NGC 3516 is potentially a good laboratory for studying the interaction between the active nucleus and the host galaxy. Classified as SB0 (Sandage & Tammann 1987), it is expected to have a relatively low-density interstellar medium compared with later type spirals, with which the majority of Seyfert galaxies are associated. Thus contamination of the nuclear radio continuum and optical line emission by supernova remnants and H II regions,

either circumnuclear or in spiral arms, should not be a major problem in this galaxy. Further, if the interstellar density is low, we might expect the radio plasma and ionizing photons to propagate farther from the nucleus, creating a radio source and emission-line nebulosity which are larger than in galaxies with denser interstellar media. At a distance of 38 Mpc (assuming a heliocentric recession velocity of 2664 km s^{-1} [Sandage & Tammann 1987], a recession velocity with respect to the velocity centroid of the Local Group of 2838 km s^{-1} and a Hubble constant of $75 \text{ km s}^{-1} \text{ Mpc}^{-1}$), NGC 3516 is one of the nearer Seyfert galaxies and can be investigated with good linear resolution ($1'' = 180 \text{ pc}$).

Previous high-resolution VLA “snapshot” observations at 20, 6, and 2 cm detected only an unresolved source coincident with the optical nucleus (Ulvestad & Wilson 1984b, 1989). Wrobel & Heeschen (1988) have made a more sensitive VLA map at 6 cm with resolution $7.5 \times 4.8''$ and found a linear structure extending about $20''$ (3.7 kpc) toward the northeast with a possible indication of weak counterstructure to the southwest of the nucleus. An extended line emission nebulosity is observed on the kpc scale. Ulrich & Péquignot (1980) showed that the intensities of the emission lines in this nebulosity are well explained by a photoionization model with a power law spectrum for the ionizing radiation. A kinematic study of this nebulosity was conducted by Goad & Gallagher (1987).¹ Their long-slit spectrum in p.a. 37° is inconsistent with purely circular motion and is suggestive of a bipolar outflow (with the gas to the NE of the nucleus flowing toward us) at velocities of the order of the escape velocity from the galaxy. Pogge (1989) has imaged NGC 3516 in the light of [O III] $\lambda 5007$ and $\text{H}\alpha + [\text{N II}] \lambda\lambda 6548, 6584$, finding a bipolar nebulosity aligned NE-SW with a size of $\approx 20''$ ($\approx 3.7 \text{ kpc}$). He also estimated the flux of ionizing radiation at Earth from ultraviolet data taken by the *IUE* satellite and soft X-ray data from the *Einstein Observatory*. Pogge (1989) compared this ionizing flux along our line of sight with the ionizing radiation necessary to account for the $\text{H}\alpha$ flux deduced from his image, and found no significant difference. This procedure provides no evidence for anisotropy in the ionizing radiation in NGC 3516, unlike the case in some Seyfert 2 galaxies (Wilson, Ward, & Haniff 1988).

In view of the clear evidence for “linear” radio structure in NGC 3516, we felt that a radio study with higher spatial resolution than available to Wrobel & Heeschen (1988) was warranted. We have also obtained emission-line images which are somewhat deeper and of higher resolution than Pogge’s (1989). In § 2, we briefly outline the procedures used in the observations and data reduction. § 3 presents the radio and emission-line maps and describes their morphological features. Implications are discussed in § 4, while conclusions are summarized in § 5.

2. OBSERVATIONS AND DATA REDUCTION

2.1. The Radio Maps

The VLA² observations of NGC 3516 were made in the “A” configuration at 20 and 6 cm on 1989 January 20 with approximate integrations on NGC 3516 of 2.7 and 3.9 hr, respectively.

¹ As pointed out by Goad & Gallagher (1988), “NE” and “SW” should be interchanged in Goad & Gallagher (1987). We use the corrected orientation in the present paper.

² The VLA is a facility of the National Radio Astronomy Observatory, which is operated by Associated Universities Inc., under contract with the National Science Foundation.

Each band consists of two contiguous channels with a total bandwidth of 100 MHz centered at 1489 and 4860 MHz. The data were calibrated using calibration sources observed between the integrations on NGC 3516. The calibrated data were self-calibrated, mapped, and CLEANed to give the final images.

There is a strong, unrelated source 4.3 away from NGC 3516 in p.a. = 110° . The apparent flux of this source at 20 cm is $\sim 300 \text{ mJy}$, but its true flux must be much larger in view of the heavy attenuation and radial smearing by the delay envelope. The sidelobes of this confusing source have been reduced by finding CLEAN components in two fields, one containing NGC 3516 and the other the confusing source. Because of the very strong distortion by delay envelope effects (e.g., Thompson 1988), the sidelobes of this source cannot be completely removed. Mainly for this reason, the r.m.s. noises on the final maps are 0.063 and $0.040 \text{ mJy beam}^{-1}$ at 20 and 6 cm, respectively, which values are higher than those expected on the basis of receiver noise alone ($0.020 \text{ mJy beam}^{-1}$ at 20 cm and $0.014 \text{ mJy beam}^{-1}$ at 6 cm).

2.2. The Optical Maps

The optical images were taken using a blue-coated GEC CCD camera attached to the TAURUS II Fabry-Perot interferometer (used in imaging mode, without etalon) at the Cassegrain focus of the 4.2 m William Herschel Telescope³ at the Observatorio del Roque de los Muchachos. The scale and field of view were 0.27 pixel^{-1} and $104'' \times 156''$, respectively (these values correspond to the TAURUS f/4 camera used during the observations). Images were taken through narrow-band filters centered at the redshifted wavelengths of [O III] $\lambda 5007$ and $\text{H}\alpha$ and at nearby wavelengths free of emission lines. The continuum images (“off-band”) were then subtracted from the line images (“on-band”) to provide continuum-free images in the emission lines. The $\text{H}\alpha$ image also includes [N II] $\lambda\lambda 6548, 6584$, although the $\lambda 6584$ line is redshifted longward of the 50% peak transmission wavelength. The point spread function FWHM was 1.10 ± 0.03 . An observing log is given in Table 1, while further details of the observing and reduction techniques may be found in Pérez-Fournon & Wilson (1990).

3. RESULTS AND ANALYSIS

3.1. The Radio Intensity Maps

Figure 1a shows the full resolution ($1.08 \times 1.04 \text{ FWHM}$) 20 cm map, while Figure 1b is the 6 cm contour map for the same region convolved to the same beam. In order to show faint features, the lowest plotted contour is close to the r.m.s. noise level in these maps. The brightest radio source in each map

³ The William Herschel Telescope is operated on the island of La Palma by the Royal Greenwich Observatory in the Spanish Observatorio del Roque de los Muchachos of the Instituto de Astrofísica de Canarias.

TABLE 1
LOG OF OPTICAL OBSERVATIONS

Image	Date	Filter Peak/Width (Å)	Exposure (s)
[O III] off	1988 Mar 18	5700/490	120
[O III] on	1988 Mar 18	5052/20	1200
H α off	1988 Mar 20	6230/470	120
H α on	1988 Mar 20	6607/53	480

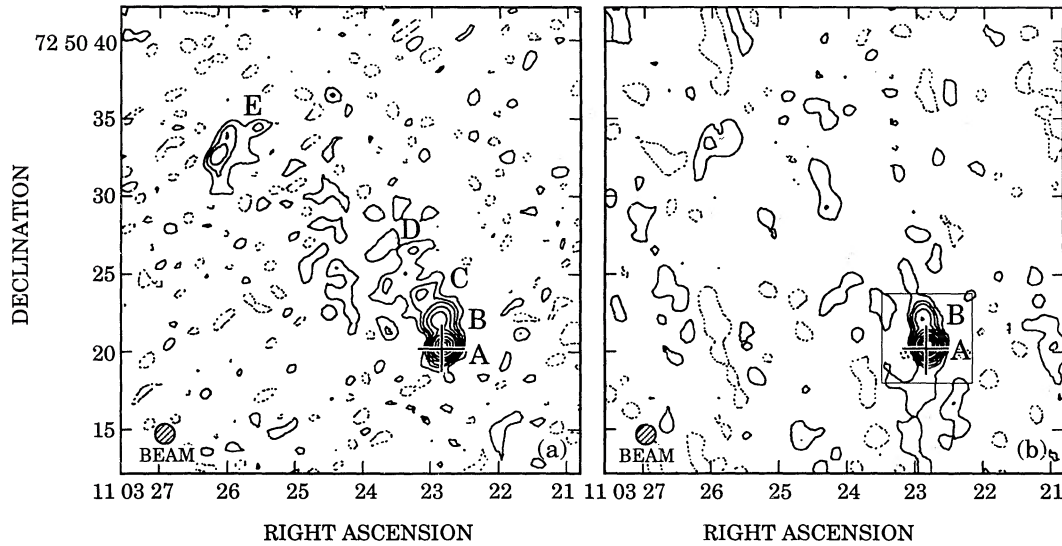


FIG. 1.—(a) A contour map of the 20 cm full resolution image. Contour values are $0.1 \times (-1, 1, 2, 3, 5, 8, 12, 20, 28, 36)$ mJy beam $^{-1}$. Beam FWHM is $1''.08 \times 1''.04$. Individual features are labeled A–E. (b) A contour map of the 6 cm image convolved to the same beam as (a). Contour values are $0.05 \times (-1, 1, 2, 3, 5, 8, 12, 20, 28, 36, 44)$ mJy beam $^{-1}$. The region corresponding to the field in Fig. 2 is indicated with a box in (b). The cross in each map shows the location of the optical nucleus (Clements 1981).

(marked A⁴ in Fig. 1a) coincides to within $0''.3$ with the location of the optical nucleus measured by Clements (1981). In the 20 cm map (Fig. 1a), the linear structure to the NE is detected showing more details than the previous 6 cm map by Wrobel & Heeschen (1988). There is a blob (B, which is also seen at 6 cm) about $2''$ north of the nucleus and probably another (C) about $2''$ further NE. Diffuse radio structure (D) extends beyond these features to about $20''$ from the nucleus. The most distant feature from the nucleus is a bow-shaped structure (E) elongated by about $2''.5$ NW–SE about $20''$ NE of the nucleus. As a whole, the NE radio structure curves toward larger p.a. with increasing distance from the nucleus. Note that the largest scale structure visible to the VLA is determined by the minimum spacings of the array and is typically $10''$ at 6 cm and $38''$ at 20 cm for “A” configuration. Figure 2 shows the central $\approx 5''$ field centered on the nucleus at 6 cm full resolution ($0''.31 \times 0''.31$ FWHM). In this map, the blob $2''$ north of the nucleus is spatially resolved and is elongated in the NW–SE direction.

3.2. Fluxes and Sizes of the Radio Components

Fluxes have been calculated for the five components marked A–E in Figure 1a. To obtain sizes and fluxes of components A–C at 20 cm and of A and B at 6 cm, an elliptical Gaussian fit program was used. The 20 cm fluxes of the extended regions D and E were evaluated by integration over the full resolution image, and the errors in these fluxes were estimated using

$$\sigma_{\text{int}} = \left[\left(\sigma \sqrt{\frac{\text{Source area}}{\text{Beam area}}} \right)^2 + (0.01 S_{\text{int}})^2 \right]^{1/2}, \quad (1)$$

where σ is the rms noise per beam given in § 2.1, and S_{int} is the total flux. The true errors may be somewhat larger than estimated in this manner, because of residual, spurious features resulting from incomplete subtraction of the background source. The results of the measurements are summarized in Table 2.

⁴ We use letters and numbers to signify radio and emission-line features, respectively.

The 20 cm and 6 cm total fluxes are compared with previous measurements in Table 3. Van der Kruit’s (1971) 21 cm flux, obtained with a $23''$ beam, is significantly larger than ours, presumably because of the insensitivity of our present observations to large-scale radio emission. The VLA snapshot observations by Ulvestad & Wilson (1984b) detected only component A at 6 cm and component A plus possibly B at 20 cm. Their 20 and 6 cm fluxes agree reasonably well with our fluxes from these components. The 6 cm observation of Wrobel & Heeschen (1988) was much more sensitive to diffuse emission than ours, so their flux is much higher than the present 6 cm measurement. Wrobel & Heeschen’s (1988) peak flux of ≈ 4 mJy beam $^{-1}$ agrees reasonably well with the sum of the fluxes of components A and B in our 6 cm map.

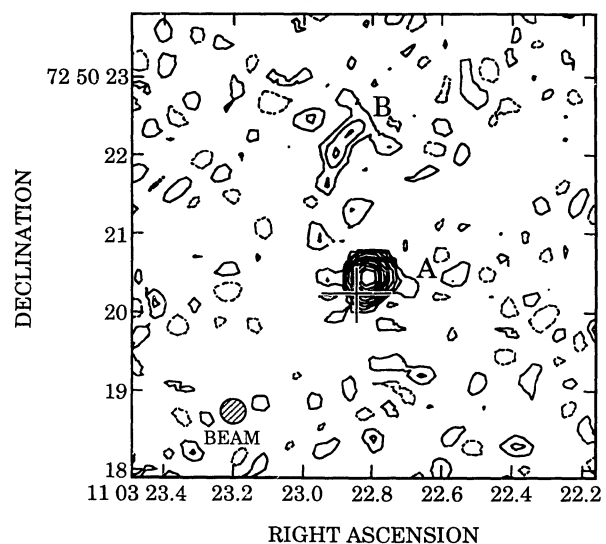


FIG. 2.—A contour map of the 6 cm full resolution image for the central region ($\sim 6'' \times 6''$). Beam FWHM: $0''.31 \times 0''.31$. Contour values are $0.05 \times (-1, 1, 2, 3, 5, 8, 12, 17, 23, 30, 38)$ mJy beam $^{-1}$. The cross shows the location of the optical nucleus. Features A and B are labeled as in Fig. 1.

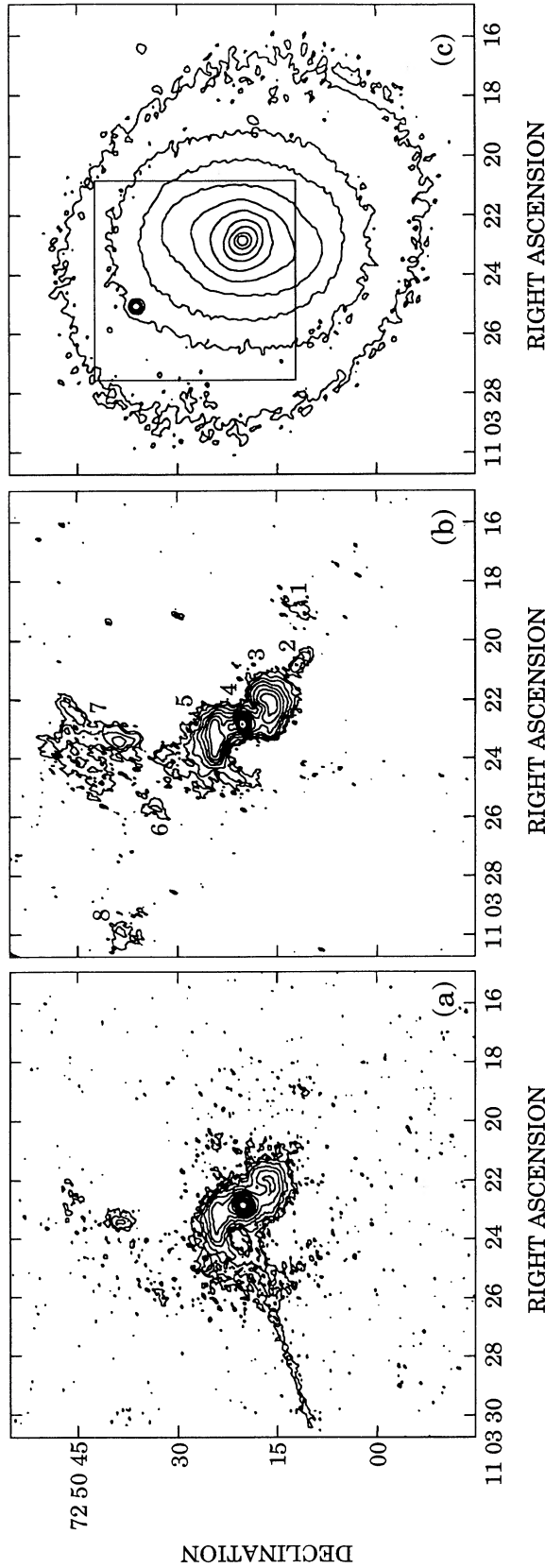


FIG. 3.—Contour maps of emission-line and optical continuum images. They have not been flux-calibrated. (a) $H\alpha + [N II] \lambda\lambda 6548, 6584$ line emission. The very narrow feature extending from the nucleus to the lower left-hand edge of the map is spurious (due to a hardware problem, which resulted in the CCD being read out while the TAURUS shutter was still open), and does not represent real line emission. (b) $[O III] \lambda 5007$ line emission. Features are labeled 1–8. Contour values for (a) and (b) are 10×2^n counts pixel^{-1} , where n takes integers between 0 and 11 in (a) and between 0 and 10 in (b). (c) Continuum emission (5700 Å). Contour values are $6.6 + (20 \times 2^n)$ counts pixel^{-1} above sky background, where n takes integer values between 0 and 9. The region corresponding to the field in Figs. 1a and 1b is indicated with a box.

TABLE 2
SUMMARY OF RADIO IMAGE ANALYSIS

COMPONENT	FLUX (mJy)		SIZE (after deconvolution from Gaussian beam)	AREA OF FLUX INTEGRATION
	6 cm	20 cm		
A	2.80 ± 0.05	4.31 ± 0.07	$< 0''.1^a$...
B	0.64 ± 0.1	2.17 ± 0.07	1.0×0.6^b	...
C	0.46 ± 0.06	$< 1''^c$...
D	4.0 ± 0.5	...	$\approx 9'' \times 9''$
E	1.7 ± 0.3	...	$\approx 7 \times 3$

^a Gaussian fit to the 6 cm full resolution image.

^b Gaussian fit to the 6 cm image smoothed to a resolution of $0''.6 \times 0''.6$.

^c We were unable to obtain a satisfactory Gaussian fit with width as a free parameter because of the confusion problems discussed in the text. The 20 cm beam width listed was taken as a reasonable upper limit.

TABLE 3
COMPARISON OF TOTAL FLUXES (mJy)

21 cm	20 cm	6 cm	References
$22. \pm 2.$	1
...	5.0 ± 1.0	4.3 ± 0.5	2
...	...	15.5 ± 1.7	3
...	12.6 ± 0.6	3.4 ± 0.1	4

REFERENCES.—(1) van der Kruit 1971; (2) Ulvestad & Wilson 1984b; (3) Wrobel & Heeschen 1988; (4) this work.

3.3. The Emission-Line Images

The emission-line images are presented in Figure 3, along with the green continuum. As first found by Pogge (1989), the emission-line gas within $10''$ of the nucleus takes a “Z”-shaped form (features 3 and 5 on the [O III] $\lambda 5007$ image in Fig. 3) which is remarkably symmetric about the nucleus (feature 4). Pogge (1989) obtained a spectrum $8''$ NE of the nucleus, revealing that this gas is of high excitation and is presumably photoionized by the active galactic nucleus. Although only an approximate flux ratio $F([\text{O III}] \lambda 5007)/F(\text{H}\alpha + [\text{N II}] \lambda \lambda 6548, 6584)$ distribution can be constructed from our images, it is clear that most of the extended gas visible in Figure 3 is of high excitation. While more spectrophotometric measurements of line ratios are desirable, we shall, in the rest of the paper, assume that all the gas is ionized by the nucleus and not by hot stars in H II regions. There are a number of features, marked 1, 2, 6, 7, and 8 on the [O III] $\lambda 5007$ image in Figure 3, at larger distances from the nucleus than the “Z”-shaped emission. The most extensive of these is feature 7 (located between $15''$ and $30''$ N of the nucleus), the southern part of which is elongated along the direction to the nucleus. More remarkably, features 2 and 6 are precisely aligned across the nucleus, as are features 1 and 8. Ignoring feature 7, there is a clear trend for the p.a. of the line emitting features (with respect to the nucleus) to increase with increasing distance from the nucleus on both the NE and SW sides. Most of these [O III] $\lambda 5007$ features are seen more weakly on the $\text{H}\alpha + [\text{N II}] \lambda \lambda 6548, 6584$ image, but there are no counterparts in the continuum picture (Fig. 3). The interpretation of the emission-line morphology is discussed later in § 4.2.

3.4. Comparison of Radio Continuum and Optical Emission-Line Maps

Figure 4 shows the [O III] $\lambda 5007$ emission-line contour map overlaid on the gray-scale 20 cm map. This overlay was

achieved by means of the astrometric optical (Clements 1981) and radio positions of the continuum nucleus. The uncertainty in the rotation of the optical images is about 1° – 2° and their linear scale is believed accurate to about 1%. Figures 1–4 reveal the following relationships between the radio continuum and optical emission line distributions.

1. The radio structure is one-sided while the emission-line structure is two-sided and shows a high degree of symmetry about the nucleus.

2. A hot spot is clearly apparent in the [O III] $\lambda 5007$ image at the position of radio feature B, some $2''$ N of the nucleus. There is also a hint of this hot spot in the $\text{H}\alpha + [\text{N II}] \lambda \lambda 6548, 6584$ image. No corresponding feature is seen in the optical continuum image.

3. Radio components C and D correspond quite well to the NE side of the “Z”-shaped emission-line structure (feature 5). The detailed association is hard to assess because of the faintness of these radio components.

4. Feature 6 in the [O III] $\lambda 5007$ emission-line image lies adjacent to, and about $1''.5$ W of, radio component E. These line and radio continuum sources are both elongated NW-SE, which direction is roughly perpendicular to the direction to the nucleus.

4. DISCUSSION

4.1. Optical Polarization and the Present Nuclear Axis of NGC 3516

Antonucci (1983, 1984) has found that the nuclear optical continuum polarization vector tends to align with the radio source in Seyfert 1 galaxies. Thompson et al. (1980) have reported optical polarizations of $p = 0.95\% \pm 0.16\%$ with p.a. = $5^\circ 9' \pm 4^\circ 9'$ at 4400 \AA and $p = 0.65\% \pm 0.09\%$ with p.a. = $178^\circ \pm 3^\circ 9'$ at 5900 \AA for the nucleus of NGC 3516. A typical Galactic foreground polarization toward NGC 3516 is $\leq 0.2\%$, and the polarization is likely to be intrinsic to the nuclear region of NGC 3516 (also R. R. J. Antonucci, private communication). Our high-resolution radio maps (Figs. 1 and 2) show that component B lies in p.a. $\approx 10^\circ$ with respect to the nucleus and defines the smallest scale ($\approx 2''$) radio axis. Further, the [O III] $\lambda 5007$ image has a similar alignment on the $2''$ scale (Figs. 3 and 4). We can thus conclude that the present nuclear ejection axis in NGC 3516 falls in p.a. $\approx 0^\circ$ – 10° .

Brindle et al. (1990) do not confirm the trend for the radio structural axis and the optical polarization vectors to align in Seyfert 1's. Their result may be a consequence of using the p.a. of the larger scale radio emission, rather than that very close to the nucleus, or of contamination of the nuclear optical polar-

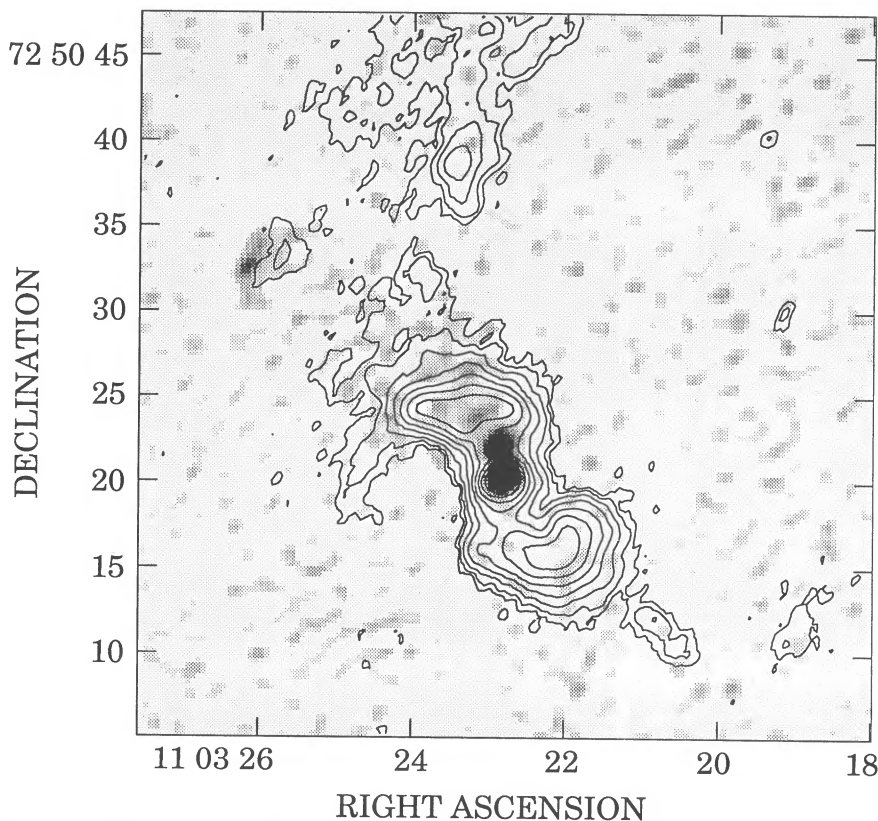


FIG. 4.—A gray-scale representation of the 20 cm full resolution image overlaid on a contour map of the [O III] $\lambda 5007$ image. Gray-scale flux range: $0.05\text{--}0.5$ mJy beam $^{-1}$. The [O III] $\lambda 5007$ image has not been flux-calibrated. Contour levels are logarithmic, with the flux ratio between successive contours equal to 2.

ization by subsequent propagation through aligned grains in the galaxy disks or the Milky Way. Since the optical polarizations in Seyfert 1 galaxies are weak and can easily be contaminated by these processes, it is important to assess each case individually. In NGC 3516, it appears that the optical polarization is intrinsic to the Seyfert nucleus and aligned with the radio ejection axis.

4.2. Radio and Emission-Line Morphologies

In this subsection, we shall discuss some aspects of the gaseous morphologies of NGC 3516, especially (1) the fact that the radio structure is almost completely one sided, while the emission-line morphology shows a high degree of symmetry about the nucleus, (2) the bending of the radio structure and the “Z”-shaped morphology of the line emission, (3) the morphological evidence for ejecta-driven radiative bow shocks, and (4) the nature of emission-line feature 7.

4.2.1. The One-sided Radio Emission

Possible explanations for the one-sided radio structure are as follows: (1) The ejection is intrinsically double-sided with the plasma traveling at a relativistic or subrelativistic speed, so the jet flowing toward us is brightened by relativistic effects, as is believed to be the case in powerful radio galaxies. (2) The interstellar media are different on the two sides, leading to an enhanced efficiency of radio emission production to the NE. (3) The ejection is intrinsically one-sided. The existence of a hot spot in the emission-line images at the position of radio component B might suggest that the line-of-sight velocity of this radio knot is within the velocity width of the narrow-band filters through which the emission-line images were taken

($\approx \pm 500$ km s $^{-1}$). This would rule out explanation (1) if the radio and line-emitting plasma share the same kinematics. It is likely, however, that the radio emission arises through interaction of a “jet” with an external cloud, in which case the velocities of the radio-emitting flow and the associated line-emitting gas may be different. In this galaxy, the NE side of the emission-line nebulosity, where radio emission is found, flows toward us (Goad & Gallagher 1987, 1988). This would be consistent with explanation (1) if radio plasma and line-emitting gas escape from the nucleus in the same direction, presumably along the rotation axis of the central accretion disk. The bow shock picture of the radio emission discussed in § 4.2.3, however, is not consistent with explanation (1). The second possibility (2) cannot be ruled out completely. However, we do not favor this explanation because of the considerable degree of symmetry about the nucleus in the emission-line maps. A statistical study of the interstellar medium in the circumnuclear environment of Seyfert galaxies with one-sided linear radio structures would give clues to distinguish these explanations.

4.2.2. The Bendings of Emission-Line and Radio Structures

The “Z”-shaped structure of the emission-line gas does not correspond to any stellar structure in the underlying galaxy (Fig. 3c), confirming that the gas is ionized by the active nucleus rather than hot stars. One possible explanation for the “Z” shape is that the ionizing radiation is collimated into a beam or a narrow cone by a central, thick disk and that the “Z” shape traces the intersection of the beam with circumnuclear gas clouds as the disk precesses. If the density is as high as implied by Ulrich & Péquignot’s (1980) model M1 ($n_e \approx 30$

cm^{-3}), the short recombination time ($\approx 10^5/n_e$ yr; n_e in cm^{-3}) of the ionized gas argues against this explanation unless the precession is so rapid that the radiation cone sweeps over the clouds at speeds comparable to that of light. In the rapid precession picture, the good correspondence between the emission-line and radio structures implies that the radio plasma also travels outward relativistically (i.e., at the same speed as the ionizing photons). Alternatively, the structure may trace the (column) density of the gas while the ionizing radiation covers a wider solid angle. The gas could comprise a bipolar outflow or represent a part of a ring of ambient gas around the nucleus. In the latter case, only those parts of the ring which are illuminated by a wide cone of ionizing radiation from the nucleus would be visible in emission lines.

Since the radio structure seems to follow the emission-line gas quite well, the bending processes for the relativistic and thermal gases are probably the same, or closely connected. Wilson & Ulvestad (1982) have discussed the bending of radio "jets" in two nearby Seyfert galaxies NGC 1068 and NGC 4151. The possible bending mechanisms they considered were (i) slow precession of the collimating nozzle; (ii) differential thermal pressure across the jet due to static pressure gradients in the interstellar gas (Henriksen, Vallée, & Bridle 1981); and (iii) "sweeping" of the jet by the ram pressure of the normally rotating interstellar medium of the host galaxy. Wilson & Ulvestad (1982) argued against the second mechanism (ii) because the jets bend *away* from the minor axis of the galaxy (projected rotation axis) in both NGC 1068 and NGC 4151, contrary to the expectation for bending by static pressure gradients. The same problem exists for NGC 3516, whose major axis position angle is about 55° (de Vaucouleurs, de Vaucouleurs, & Corwin 1978; see also the continuum image in Fig. 3c). Mechanism (ii) is also much less "efficient" than (iii), because in the former process only the pressure difference across the jet thickness (which is much smaller than the total pressure) can contribute to the bending, while in mechanism (iii) essentially the whole ram pressure is available. We thus favor either mechanism (i) or (iii) as being responsible for the observed curvature. Another possibility is (iv) bending by gravitational forces in low velocity outflows, in which the gases are ejected into the galaxy halo and then fall back into the disk.

Goad & Gallagher (1987) interpreted the variation of velocity along their spectrograph slit in terms of a bipolar flow, which is decelerated by the gravitational potential of NGC 3516, and possibly falling back onto the galaxy disk. The line-of-sight velocity inversion which they found in the SW flow, and the "Z"-shaped emission line morphology (features 5, 4, and 3 in Fig. 3b) can be qualitatively understood in such a picture. The curved narrow structure elongated NW-SE, which extends from the east end of the NE lobe (feature 5 in Fig. 3b) some $8''$ east of the nucleus, is particularly suggestive of gas falling back onto the galaxy disk and even through it. On the other hand, the radio structure (features B, C, D, and E in Fig. 1) follows the bending of the emission-line gas in the NE lobe (feature 5) but seems to penetrate beyond it. This result may imply that the outflow of radio plasma is faster than the outflow of emission-line gas.

4.2.3. Nuclear Ejecta-driven Radiative Bow Shocks

Radio feature E is reminiscent of the limb-brightened northeast lobe of NGC 1068, which Wilson & Ulvestad (1987) modeled in terms of a radiative bow shock driven by a narrow jet. In this picture, the compressed magnetic field and possibly

shock-accelerated (by first-order Fermi acceleration) cosmic rays are responsible for the observed radio emission. The other off-nuclear radio components (B, C, and a part of D) show signs of being elongated perpendicular to the general outflow direction (see Fig. 1a and Fig. 2). An interesting aspect, apparent in Figure 4, is associations between some of these radio components and emission-line blobs. An emission-line blob is clearly seen at the position of B (see also Figs. 3a and 3b). Radio component E and emission line component 6 also appear to be associated, being aligned side by side with a separation of ~ 1.5 (~ 270 pc) and with the emission-line gas being closer to the nucleus. This separation can be understood if the radio emission comes from near the shock front and the emission-lines from the dense postshock cooling layer illuminated by the central ionizing radiation, as modeled by Taylor et al. (1989) (see also Pedlar, Dyson, & Unger 1985 in which the shock is driven by expansion of a radio lobe rather than outward motion). Figure 4 suggests that we can treat the observed structure as nearly plane-parallel, and the cooling length given below (Whittle et al. 1986) is a good indication of the displacement:

$$l_{\text{cool}} = 1.4 \times 10^{-9} n_a^{-1} V_s^4 \text{ pc}, \quad (2)$$

where V_s is the shock velocity in km s^{-1} and n_a is the preshock density in cm^{-3} . For $n_a = 0.01\text{--}10 \text{ cm}^{-3}$ (reasonable for the central regions of an S0 galaxy), a cooling length of 270 pc requires $V_s \approx 200\text{--}1200 \text{ km s}^{-1}$. Such shock velocities are not unreasonable given the emission-line kinematics (Goad & Gallagher 1987). Our data are not good enough to show whether there are similar displacements between the other radio continuum and emission-line features.

Figures 3a and 3b show a few clumps of line-emitting gas (features 1, 2, 6, and 8) outside the inner "Z"-shaped region (features 3 and 5). As already mentioned (§ 3.3), features 2 and 6 and also features 1 and 8 (Fig. 3b) are precisely aligned across the nucleus. Given our interpretation of feature 6 as line emission from a dense postshock cooling zone, it is reasonable to interpret features 1, 2, and 8 in the same way. These features presumably represent past, highly collimated, bipolar ejections from the nucleus, driving radiative shocks into the interstellar medium of NGC 3516. If this idea is correct, more sensitive radio maps would be expected to reveal radio emission at or near these locations. The features on the NE side of the nucleus (6 and 8) are farther from the nucleus than their partners to the SW (2 and 1), suggesting a small asymmetry in either ejection parameters or the interstellar density across the nucleus. It is noteworthy that these features follow a similar trend of increasing position angle with respect to the nucleus with increasing distance from it, so a similar process to that responsible for the inner "Z"-shaped structure (cf. § 4.2.2) is apparently influencing their trajectories.

4.2.4. Emission-Line Feature 7

A conspicuous region of high-excitation line emission not previously discussed is feature 7 (Figs. 3a and 3b). The southern part of this cloud has an elongated structure that "points" almost directly toward the nucleus. Further, the peak of feature 7 lies in p.a. $\approx 8^\circ$ with respect to the nucleus, which is in excellent agreement with the *present* nuclear axis of NGC 3516 (§ 4.1). These properties may be accounted for in terms of ionization of ambient gas by a narrow (opening angle $\lesssim 9^\circ$) beam of ionizing radiation escaping from the nucleus along its present axis. Such a beam might result from directed rela-

tivistic motion with $\gamma \gtrsim 6$ (“blazar-like” beam) or an unusually narrow funnel in a radiation pressure-supported accretion torus (e.g., Madau 1988). This possible narrow beam in NGC 3516 is misaligned with respect to our line of sight and shows up only through its ionization of interstellar gas. A similar situation has recently been found in Cen A by Morganti et al. (1990). We consider the alternative explanation, that the elongated morphology of feature 7 represents the intrinsic distribution of interstellar gas rather than that of the ionizing photons, to be ad hoc and unsatisfactory. A search for similar evidence for possible misdirected “blazars” in other active galaxies would be well worthwhile.

4.3. Nature and Energetics of the Radio Emission

Spectral indices between 20 and 6 cm ($\alpha_6^{20}: F_\nu \propto \nu^{-\alpha}$) have been calculated for the radio components A and B. The nucleus (A) has a spectral index $\alpha_6^{20} = 0.36$ while the blob (B) has $\alpha_6^{20} = 1.02$. The spectral index of the nucleus calculated from the fluxes observed by Ulvestad & Wilson (1984b) is $\alpha_6^{20} \approx 0.13$. Our data suggest a steeper spectrum for the nucleus, indicating it is at least partially optically thin. Using Ulvestad & Wilson’s (1989) 2 cm flux of 1.3 ± 0.2 mJy (which probably refers to only the nuclear source) and our nuclear flux at 6 cm, the spectral index between 2 and 6 cm is $\alpha_6^2 = 0.70$. Thus, if the source has not varied between the two epochs of observation, the nucleus has a steep spectrum between 2 cm and 6 cm.

Equipartition magnetic field strengths for radio components B–E have been estimated. We have assumed a power-law spectrum with $\alpha = 1.0$ between lower and upper cutoffs of 10 MHz and 100 GHz and a value of 2 for the ratio of the total cosmic-ray energy density to the relativistic electron energy density. The results are summarized in Table 4. If the radio-emitting regions are actually thin shells, the equipartition fields would be larger than the values given. For the typical field of 2×10^{-5} G, the relativistic pressure is $P_{\text{rel}} \approx 3 \times 10^{-11}$ dyn cm $^{-2}$. In modeling the extended nebulosity, Ulrich & Péquignot (1980) favored a model (referred to as M1) with $n = 30$ cm $^{-3}$ and $T_e = 10^4$ K, implying $P_{\text{th}} \approx 4 \times 10^{-11}$ dyn cm $^{-2}$. These values of P_{th} and P_{rel} are in good agreement, suggesting an approximate pressure equilibrium between relativistic and thermal gases in the extended nebulosity. The total energy of the off-nucleus radio-emitting region (magnetic field and relativistic particles) estimated using the assumptions above is $\approx 10^{53}$ ergs. The $\text{H}\alpha + [\text{N II}] \lambda\lambda 6548, 6584$ flux of the extended nebulosity is 1.3×10^{-12} ergs cm $^{-2}$ s $^{-1}$ and about 40% of this flux is from $\text{H}\alpha$ (Pogge 1989). The total $\text{H}\alpha$ luminosity from the extended nebulosity in NGC 3516 is then 9×10^{40} ergs s $^{-1}$, corresponding to a total mass of ionized gas of 10^7 ($n/30$ cm $^{-3}$) $^{-1} M_\odot$, assuming $T = 10^4$ K. Thus the total kinetic energy of the emission-line nebulosity, flowing with a speed of ≈ 150 km s $^{-1}$ (Goad & Gallagher 1987), can be estimated at

$\approx 10^{54}$ ($n/30$ cm $^{-3}$) $^{-1}$ ergs, about an order of magnitude larger than the total energy of the relativistic component. Given the uncertainties in both calculations, we can only say that the total energies of relativistic and thermal gases are comparable to one or two orders of magnitude. A more complete discussion of the emission-line kinematics of NGC 3516 will be given in a future paper (Mulchaey et al. 1992).

5. CONCLUSIONS

From our high-resolution radio continuum and optical emission-line images of NGC 3516, we have reached the following conclusions.

1. NGC 3516 contains a linear radio structure extending over about 4 kpc. This radio emission is aligned and coplanar with the emission-line nebulosity, as is usually the case for such radio sources in Seyfert galaxies. The nuclear radio source coincides with the optical nucleus. In contrast with the emission-line nebulosity, the extended radio emission is found on only one side (the NE) of the nucleus. The physical reason for this one-sided structure is unclear.

2. The emission-line nebulosity is of high excitation and presumably photoionized by the nucleus. The nebulosity within 1.8 kpc of the nucleus has a “Z”-shaped morphology, which is remarkably symmetric about the nucleus. Further out, five more clouds of ionized gas has been found. With one exception, the p.a. of these clouds with respect to the nucleus increases with increasing distance from the nucleus, like the “Z”-shaped nebulosity closer in. The radio emission follows closely this “Z”-shaped gas morphology on the NE side, and there are detailed associations between radio and emission-line knots. This curvature of the radio and emission-line structures may reflect either bending by the ram pressure of the rotating interstellar gas, or gravitationally induced trajectories in a low-velocity outflow, or precession of the nuclear axis.

3. The position angles of the radio continuum and optical line emission on the smallest resolved scale (≈ 400 pc) both agree well with the optical polarization vector, as has been found for Seyfert 1 galaxies in earlier surveys. This direction defines the current nuclear axis. In comparing radio axes with optical polarization directions in active galaxies, it is important to use the smallest scale radio structure and to eliminate cases in which the observed optical polarization is dominated by propagation through aligned grains in the disk of the host galaxy or the Milky Way, rather than reflecting the true intrinsic nuclear polarization.

4. The linear radio structure is largely composed of a number of separate “blobs” rather than a smooth continuous structure. Several of these “blobs” are elongated *transverse* to the outflow direction, suggesting the radio emission originates in shocks driven by the outflow. The synchrotron emission is presumably a consequence of postshock compression of magnetic fields and acceleration of relativistic electrons at the shock fronts. A clear separation is found between one of these radio features and the associated emission-line gas. The emission-line cloud lies closer to the nucleus, suggesting the emission lines originate in dense gas in the cooling zone of a radiative shock. Overall, these results suggest sporadic, rather than continuous, ejection from the nucleus of NGC 3516.

5. One emission-line feature (feature 7 in Fig. 3b), which is 3.3 kpc from the nucleus, exhibits a linear morphology which “points” to the nucleus and aligns with the present nuclear axis. We speculate that it represents ambient interstellar gas photoionized by a narrow beam of ionizing radiation escaping

TABLE 4
EQUIPARTITION MAGNETIC FIELD STRENGTHS

Component	Estimated Volume (pc 3)	Equipartition Magnetic Field (G)
B	4×10^6	3×10^{-5}
C	$< 6 \times 10^6$	$> 3 \times 10^{-5}$
D	5×10^8	6×10^{-6}
E	4×10^7	2×10^{-5}

from the nucleus. This beam could result from relativistic effects ("blazar-like") or from collimation by a narrow funnel in a radiation pressure-supported torus. Such linear features in the ionized gas around active galactic nuclei can directly trace the presence of such narrow beams when they are not directed toward the observer.

6. The relativistic and thermal gases in much of the extended nebulosity appear to have approximately the same pressure.

This work was supported in part by NSF part AST 8719207

and NASA grant NAG 8-793 to the University of Maryland. We are grateful to the VLA and La Palma staffs, especially Peggy Perley and Peter Gray, for expert assistance with the observations. Thanks are also due to Zlatan Tsvetanov, John Mulchaey, Baltasar Vila-Vilaró, and José Acosta-Pulido for stimulating discussions. I. P. F. was supported in part by the Dirección General de Investigación Científica y Técnica. A. S. W. thanks the Graduate School, University of Maryland for a Faculty Research Fellowship during the completion of this work.

REFERENCES

- Antonucci, R. R. J. 1983, *Nature*, 303, 158
 ———. 1984, *ApJ*, 278, 499
 Antonucci, R. R. J., & Miller, J. S. 1985, *ApJ*, 297, 621
 Brindle, C., Hough, J. H., Bailey, J. A., Axon, D. J., Ward, M. J., Sparks, W. B., & McLean, I. S. 1990, *MNRAS*, 244, 577
 Clements, E. D. 1981, *MNRAS*, 197, 829
 de Vaucouleurs, G., de Vaucouleurs, A., & Corwin, H. G., Jr. 1976, *Second Reference Catalogue of Bright Galaxies* (Austin: University of Texas Press)
 Goad, J. W., & Gallagher, J. S. 1987, *AJ*, 94, 640
 ———. 1988, *AJ*, 95, 948
 Haniff, C. A., Wilson, A. S., & Ward, M. J. 1988, *ApJ*, 334, 104
 Heckman, T. M., Miley, G. K., van Breugel, W. J. M., & Butcher, H. R. 1981, *ApJ*, 247, 403
 Henriksen, R. N., Vallée, J. P., & Bridle, A. H. 1981, *ApJ*, 249, 40
 Madau, P. 1988, *ApJ*, 327, 116
 Morganti, R., Robinson, A., Fosbury, R. A. E., di Serego Alighieri, S., Tadhunter, C. N., & Malin, D. F. 1991, *MNRAS*, in press
 Mulchaey, J. S., Tsvetanov, Z., Wilson, A. S., & Pérez-Fournon, I. 1992, in preparation
 Osterbrock, D. E. 1978, *Proc. Nat. Acad. Sci.*, 75, 540
 Pedlar, A., Dyson, J. E., & Unger, S. W. 1985, *MNRAS*, 214, 463
 Pérez-Fournon, I., & Wilson, A. S. 1990, *ApJ*, 356, 456
 Pogge, R. W. 1989, *AJ*, 98, 124
 Sandage, A., & Tammann, G. 1987, *Revised Shapley-Ames Catalog of Bright Galaxies* (2d ed.; Washington D.C.: Carnegie Institute of Washington)
 Tadhunter, C., & Tsvetanov, Z. 1989, *Nature*, 341, 422
 Taylor, D., Dyson, J. E., Axon, D. J., & Pedlar, A. 1989, *MNRAS*, 240, 487
 Thompson, I., Landstreet, J. P., Stockman, H. S., Angel, R. J. P., & Beaver, E. A. 1980, *MNRAS*, 192, 53
 Thompson, A. R. 1988, in *Synthesis Imaging in Radio Astronomy* ed. R. A. Perley, F. R. Schwab, & A. H. Bridle (ASP Conf. Ser., 6), 11
 Ulrich, M.-H., & Péquignot, D. 1980, *ApJ*, 238, 45
 Ulvestad, J. S., & Wilson, A. S. 1984a, *ApJ*, 278, 544
 ———. 1984b, *ApJ*, 285, 439
 ———. 1989, *ApJ*, 343, 659
 van der Kruit, P. C. 1971, *A&A*, 15, 110
 Whittle, M. 1985, *MNRAS*, 213, 33
 ———. 1989, in *Extranuclear Activity in Galaxies* (ESO Conference and Workshop Proceedings 32), ed. E. J. A. Meurs and R. A. E. Fosbury (Garching: European Southern Observatory), 199
 Whittle, M., Haniff, C. A., Ward, M. J., Meurs, E. J. A., Pedlar, A., Unger, S. W., Axon, D. J., & Harrison, B. A. 1986, *MNRAS*, 222, 189
 Whittle, M., Pedlar, A., Meurs, E. J. A., Unger, S. W., Axon, D. J., & Ward, M. J. 1988, *ApJ*, 326, 125
 Wilson, A. S. 1987, in *IAU Symp. 121, Observational Evidence of Activity in Galaxies*, ed. E. Khachikian, G. Melnick, & K. Fricke (Dordrecht: Reidel), 237
 Wilson, A. S., & Ulvestad, J. S. 1982, *ApJ*, 263, 576
 ———. 1987, *ApJ*, 319, 105
 Wilson, A. S., Ward, M. J., & Haniff, C. A. 1988, *ApJ*, 334, 121
 Wilson, A. S., & Willis, A. G. 1980, *ApJ*, 240, 429
 Wrobel, J. M., & Heeschen, D. S. 1988, *ApJ*, 335, 677